ISSN 0915-633X

INTERNATIONAL ATOMIC ENERGY AGENCY

17th IAEA Fusion Energy Conference
Yokohama, Japan, 19 - 24 October 1998

IAEA-CN-69/ OV1/4

NATIONAL INSTITUTE FOR FUSION SCIENCE

An Overview of the Large Helical Device Project

A. Iiyoshi, A. Komori, A. Ejiri, M. Emoto, H. Funaba, M. Goto, K. Ida, H. Idei, S. Inagaki, S. Kado, O. Kaneko, K. Kawahata, S. Kubo, R. Kumazawa, S. Masuzaki, T. Minami, J. Miyazawa, T. Morisaki, S. Morita, S. Murakami, S. Muto, T. Muto, Y. Nagayama, Y. Nakamura, H. Nakanishi, K. Narihara, K. Nishimura, N. Noda, T. Kobuchi, S. Ohdachi, N. Ohyabu, Y. Oka, M. Osakabe, T. Ozaki, B.J. Peterson, A. Sagara, S. Sakakibara, R. Sakamoto, H. Sasao, M. Sasao, K. Sato, M. Sato, T. Seki, T. Shimozuma, M. Shoji, H. Suzuki, Y. Takeiri, K. Tanaka, K. Toi, T. Tokuzawa, K. Tsumori, I. Yamada, H. Yamada, S. Yamaguchi, M. Yokoyama, K.Y.Watanabe, T. Watari, R. Akiyama, H. Chikaraishi, K. Haba, S. Hamaguchi, S. Iima, S. Imagawa, N. Inoue, K. Iwamoto, S. Kitagawa, Y. Kubota, J. Kodaira, R. Maekawa, T. Mito, T. Nagasaka, A. Nishimura, Y. Takita, C. Takahashi, K. Takahata, K. Yamauchi, H. Tamura, T. Tsuzuki, S. Yamada, N. Yanagi, H. Yonezu, Y. Hamada, K. Matsuoka, K. Murai, K. Ohkubo, I. Ohtake, M. Okamoto, S. Sato, T. Satow, S. Sudo, S. Tanahashi, K. Yamazaki, M. Fujiwara and O. Motojima

(Received - Oct. 7, 1998)

NIFS-571 Oct. 1998

RESEARCH REPORT
NIFS Series

NAGOYA, JAPAN

AN OVERVIEW OF THE LARGE HELICAL DEVICE PROJECT

A. IIYOSHI, A. KOMORI, A. EJIRI, M. EMOTO, H. FUNABA,
M. GOTO, K. IDA, H. IDEI, S. INAGAKI, S KADO, O. KANEKO,
K. KAWAHATA, S. KUBO, R. KUMAZAWA, S. MASUZAKI,
T. MINAMI, J. MIYAZAWA, T. MORISAKI, S. MORITA,
S MURAKAMI, S. MUTO, T. MUTOH, Y. NAGAYAMA,
Y. NAKAMURA, H. NAKANISHI, K. NARIHARA, K. NISHIMURA,
N. NODA, T. KOBUCHI, S. OHDACHI, N. OHYABU, Y. OKA,
M. OSAKABE, T. OZAKI, B. J. PETERSON, A. SAGARA,
S. SAKAKIBARA, R. SAKAMOTO, H. SASAO, M. SASAO, K. SATO,
M. SATO, T. SEKI, T. SHIMOZUMA, M. SHOJI, H. SUZUKI,
Y. TAKEIRI, K. TANAKA, K. TOI, T. TOKUZAWA, K. TSUMORI,
K. TSUZUKI, I. YAMADA, H. YAMADA, S. YAMAGUCHI,
M. YOKOYAMA, K. Y. WATANABE, T. WATARI, R. AKIYAMA,
H. CHIKARAISHI, K. HABA, S. HAMAGUCHI, M. IIMA, S. IMAGAWA,
N. INOUE, K. IWAMOTO, S. KITAGAWA, Y. KUBOTA, J. KODAIRA,
R. MAEKAWA, T. MITO, T. NAGASAKA, A. NISHIMURA, Y. TAKITA,
C. TAKAHASHI, K. TAKAHATA, K. YAMAUCHI, H. TAMURA,
T. TSUZUKI, S. YAMADA, N. YANAGI, H. YONEZU, Y. HAMADA,
K. MATSUOKA, K. MURAI, K. OHKUBO, I. OHTAKE, M. OKAMOTO,
S. SATOH, T. SATOW, S. SUDO, S. TANAHASHI, K. YAMAZAKI,
M. FUJIWARA, O. MOTOJIMA
National Institute for Fusion Science,
Toki 509-5292, Japan

Abstract

AN OVERVIEW OF THE LARGE HELICAL DEVICE PROJECT.

The Large Helical Device (LHD) has successfully started running plasma confinement experiments after a long construction period of eight years. During the construction and machine commissioning phases, a variety of milestones have been attained in fusion engineering, which successfully led to the first operation, and the first plasma was ignited on March 31, 1998. Two experimental campaigns are planned in 1998. In the first campaign, the magnetic flux mapping clearly demonstrated a nested structure of magnetic surfaces. The first plasma experiments were conducted with second harmonic 84-GHz and 82.6-GHz ECH at a heating power input of 0.35 MW. The magnetic field was set at 1.5 T in the first year so as to accumulate operational experience of the superconducting coils. In the second campaign, auxiliary heating with NBI at 3 MW has been carried out. The averaged electron densities up to 6×10^{19} m^{-3}, central temperatures ranging 1.4 to 1.5 keV and stored energies up to 220 kJ have been attained despite the fact that impurity level is not yet minimized. The obtained scaling of energy confinement time has been found to be consistent with the ISS95 scaling law with some enhancement.

1. INTRODUCTION

The Large Helical Device (LHD) offers a great opportunity to study currentless plasmas in the heliotron configuration. LHD is a large heliotron with a major radius, R, of 3.9 m and a minor

radius, a, of 0.65 m [1-4]. Full steady-state operation is expected, using superconducting coils in addition to full helical divertor. Steady-state plasma operation, essential to magnetic fusion reactors, is an inherent advantage of heliotrons over tokamaks, and can be realized with the full helical divertor because it removes heat flux form the core plasma and controls impurity recycling. However, since the closed full helical divertor will not be ready in the near future, we plan to use a local island divertor (LID) for the LHD edge plasma control [5, 6]. LID is a closed divertor that uses an m/n = 1/1 island. The technical ease of hydrogen pumping is the advantage of LID over the closed full helical divertor because hydrogen recycling is toroidally localized [5, 6].

The eight-year construction phase has led to a successful engineering commissioning of the device. Figure 1 shows a picture of LHD taken in the second campaign. The basic physics objectives are [1]: (1) to produce high $n\tau$ T currentless plasmas and study transport issues to obtain basic data which can extrapolated to the reactor-grade plasma, (2) to achieve high-β plasma with $<\beta> >5\%$ and study related physics, (3) to install a divertor and obtain basic data for steady-state operation, (4) to study the behavior of high-energy particles in the heliotron magnetic field and conduct simulation experiments of alpha particles in reactor plasmas and (5) to promote complementary studies to tokamak plasmas to increase understanding of magnetically confined toroidal plasmas. Engineering R&D experiences have also contributed to advance in fusion technology. LHD employs a pair of l/m = 2/10 helical coils (liquid helium pool cooled), three sets of poloidal coils (super-critical helium forced-flow cooled) and nine pairs of bus lines (two-fluid helium forced-flow cooled). The mass at the cryogenic temperature of 4.4 K is 822 tons. The transition to the superconducting state has been achieved after 4 weeks for cooling of coils.

Initial plasma experiments have started with second harmonic 82.6 GHz and 84 GHz ECH of 0.35 MW at 1.5 T. NBI of 3 MW with negative ion sources, optimized for low energy of 100 keV, has been applied in the second campaign. This paper is intended to present an overview of the LHD project, including the construction procedure, associated technology R&D activities, the plasma

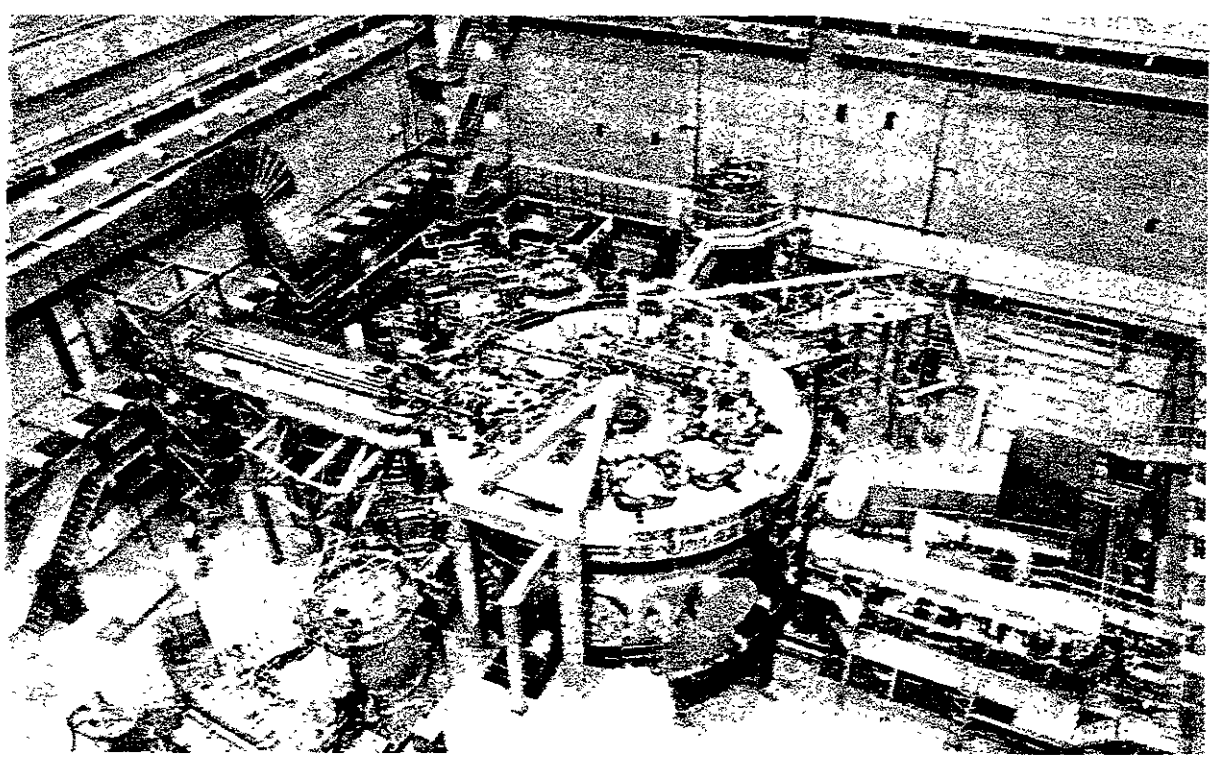

FIG. 1. Photograph of LHD taken during the second campaign.

TABLE I. SPECIFICATIONS OF LHD

Items	Phase I [II]
Major radius (R)	3.9 m
Minor radius (a)	0.65 m
Plasma volume (V_p)	30 m^3
Coil minor radius (a_c)	0.975 m
Magnetic field (B_t)	3 [4] T
Magnetic energy	0.9 [1.6] GJ
Heating power	
ECH	10 MW
NBI	15 [20] MW
ICRF	3–12 MW
Target plasma	
T_i	> 10 keV
$n\tau_E T_i$	> 10^{20} keVm^{-3} s
β	> 5%

confinement experiments in the first campaign, the updated results from auxiliary heating experiments with NBI in the second campaign, future plans and so on.

2. ADVANCED TECHNOLOGY

The specifications of LHD are shown in Table I. Notice that we have two operational regimes for LHD. In Phase-I, the helical magnetic field is set at 3 T, whereas the field will be increased to 4 T in Phase-II.

Along with the design and construction efforts, tremendous amount of knowledge has been obtained in the areas of cryogenic engineering, plasma facing components and so on. This report is intended to summarize the main results in the cryogenic engineering, plasma heating devices and diagnostics. The detail technology R&D is presented elsewhere [7].

2.1. R&D of superconducting coils

The specifications of coil-sets are listed in Table II. The poloidal coil system includes the following three sets, inner vertical (IV), inner shaping (IS) and outer vertical (OV) coils, all of which are superconducting. The bracketed parameters in Table II represent those in Phase-II.

For attaining high accurate helical shaping and winding, we selected pool-cooled medium size conductors for the helical coils. After many short sample tests [8], the final size was chosen to be 12.5 mm × 18.0 mm, and the nominal current is 13.0 kA at 4.4 K for the 3 T operation. The main stabilizer is made of pure aluminum. The conductor size was optimized not only for the mechanical flexibility for winding but also for the high cryogenic stability. In order to reduce the magnetoresistance caused by the Hall current, the aluminum structure is clad by Cu-2%Ni while maintaining a smooth current transfer from superconducting strands [9].

The cable-in-conduit conductors are used for the poloidal coils because of their high strength and rigidity against large electromagnetic forces. The void fraction was optimized from the view

TABLE II. MAJOR PARAMETERS OF SUPERCONDUCTING COILS

Items	Helical coil	IV coil	IS coil	OV coil
Major Radius (m)	3.90	1.80	2.82	5.55
Weight per coil (ton)	120	16	25	45
Magnetic stored energy (GJ)	0.92 [1.64]	0.16	0.22	0.61
Coil current density (A/mm^2)	40 [53]	29.8	31.5	33.0
Magnetomotive force (MA)	5.85 [7.8]	5.0	-4.5	-4.5
Number of turns	150×3	240	208	144
Conductor length (km)	36	2.7	3.7	5.0
Voltage to earth (kV)	±1.18 [±1.57]	±1.62	±1.75	±1.87
Cooling method	Pool-cooled	Forced flow	←	←
Number of flow paths	20	16	←	←
Length of a flow path (m)	3.9	170	230	314
Coil temperature (K)	4.4 [1.8]	4.5–4.8	←	←
Hoop force (MN)	356	262	116	263
Vertical force (MN)	240	-60.2	95.6	72.2

point of strand movement and inter-strands coupling losses. The strands surface is uncoated to maintain current redistribution and heat transfer to the coolant. We confirmed with a mock-up coil that the bare strands provide a high-stability margin during steady-state operation [10].

The superconducting flexible bus-line was developed for the current feeding system. An aluminum-stabilized compacted strands cable was developed to achieve full cryostability for 32 kA. A pair of conductors is pulled into the 50 m-long coaxial corrugated tubes. We constructed a 20 m-long full-scale mock-up. Performance tests were carried out, and we confirmed that the minimum propagating current is higher than 32.5 kA and that the current up to 40 kA can flow without quenching [11].

2.2. R&D in cryogenic engineering

The cryogenic engineering R&D includes; (1) a winding device and technique for superconducting helical coils to achieve a high dimensional accuracy [12], (2) a winding technique for cable-in-conduit conductors, (3) materials and the welding technique for a thick (100 mm) structure of SUS316 for cryogenic use [13], (4) a new coil protection circuit with a fuse [14] and (5) an advanced control system for the cryogenic system, using VME controllers and workstations [15].

2.3. R&D of plasma heating devices

The plasma heating devices using the ECH, NBI and ICRF techniques are procured for LHD experiments.

We use ECH for plasma production and electron cyclotron resonance heating with gyrotrons at the characteristic frequencies of 84 GHz, 82.6 GHz and 168 GHz. The 168 GHz gyrotron has been designed to be operated at steady state. The R&D results were that the output power of the 84 GHz gyrotron is 0.45 MW for 10.2 s and 0.5 MW for 2 s and that of the 168 GHz gyrotron is 0.5 MW for 1 s. The ECH power is injected through two ports in the first and second campaigns, and two transmission lines are installed in each port. The elliptical Gaussian beam is focused on the equatorial plane and the focal point can be changed radially and toroidally.

Two negative-ion-based NBI's are the main heating devices, and aligned for tangential injection in opposite directions (co- and counter-injection). Each NBI was designed for injecting a 7 5 MW hydrogen beam at an energy of 180 keV for 10 s by two ion sources. One of the two NBI's was also designed to inject a 100 keV, 0.5 MW beam up to 90 s. In R&D, the extracted negative ion beam current reached 25 A, passing half way to the goal value of 40 A, with the beam divergence of 10 mrad in the test ion source.

An ICRF heating system has been also developed. The 25 - 100 MHz variable high power cavity was developed for steady-state ICRF heating with a total power of 3 MW, and two kinds of wave launchers were prepared for the second and third campaigns. These launchers include a 1 MW class half turn antenna for fast wave heating and a 0.5 MW class folded wave guide for Ion Bernstein Wave heating.

2.4. Plasma vacuum vessel and density control

The plasma vacuum vessel is located inside the helical coils and helically twisted. In order to maintain high accuracy in constructing the helical coils, it was decided that the plasma vacuum vessel was assembled after the installation of the helical coils. Thus, the plasma vacuum vessel was divided into 140 parts. The joint welding was carried out after whole parts were installed. Water cooling pipes were welded on the vessel surface, facing plasmas.

Water-cooled divertor plates will be installed at the divertor strike-point areas after the second experimental campaign. Baffle plates are to be installed to form the closed full helical divertor, and a toroidal pump along four divertor-legs will be installed near the divertor plates for density control. The carbon-sheet pump [16] and membrane pump [17] have been evaluated for this purpose. The plasma vacuum vessel is to accommodate these pumps in a dumbbell-shape cross section.

2.5. R&D of Heavy ion beam probe

A heavy ion beam probe has been designed for potential profile measurements in LHD [18]. Because of the large plasma and high magnetic field in LHD, a heavy ion beam such as gold needs to be accelerated as high as 6 MeV to penetrate the plasma. The beam should have a small energy spread, and hence, a negative ion source of the plasma sputter type has been developed. Negative ions are accelerated in a tandem manner at first, and are converted into positive ions through a stripping gas cell which is at the high voltage end. A test stand has been constructed to study the negative ion production, extraction, energy dispersion and charge stripping efficiency.

2.6. Overview of construction and assembling flow

The emphasis was on keeping the work quality high during the construction, based on the following principles; (1) technology innovations were encouraged; and (2) the National Institute for Fusion Science (NIFS) was responsible for the final device performance, reducing the manufacturers' cost.

The detailed design started in 1990 and parts construction in factory started in 1991. Due to the long lead time, the production of superconducting coils was initiated immediately from the production of superconducting wires. The on-site construction of LHD started in 1994 following the completion of the housing building. Finally, the LHD construction was completed at the end of 1997.

<Supporting strucurse for coils>	
Thickness of shell	100 mm
Weight	390 ton
Material	SUS316
Cooling channel	attached pipes
<Cryostat vessel and base>	
Diameter and height	13.5 × 8.8 m
Volume	580 m^3
Weight (vessel / base)	350 / 200 ton
Material of vessel	SUS304
Material of base	manganese steel
Thickness of vessel	50 and 100 mm
Number of ports	95
<Cryogenic post>	
Load (cryogenic mass)	822 ton
Displacement by cooling	13 mm
Earthquake	0.3 G
Material	CFRP, SUS316
Heat input (to 4 / 80 K)	30 / 600 W

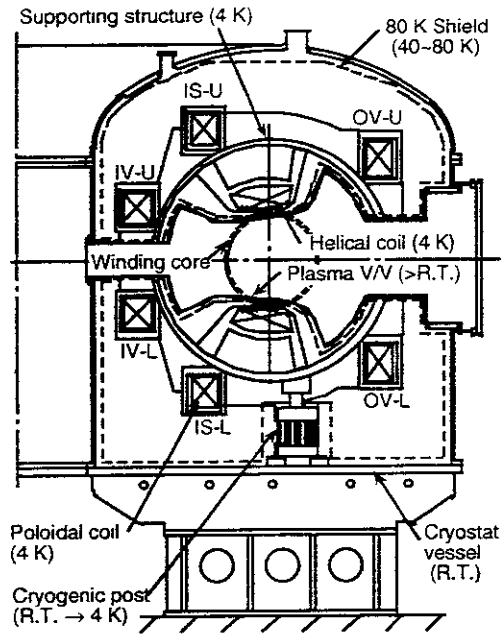

FIG. 2. Specifications and cross section of the cryostat.

The specifications and cross section of cryostat are shown in Fig. 2. Since the electromagnetic force is large, the helical coil conductors are packed into thick stainless steel cases (HC cans) that are supported from 100 mm thick supporting structures. The assembling flows of the major components were as follows; (1) to assemble the HC cans on a winding core, (2) to wind helical-coil conductors in the cans, (3) to assemble the top covers on the HC cans, (4) to assemble the outer parts of the plasma vacuum vessel between the helical coils tentatively, (5) to set the lower poloidal coils and the lower half of the supporting structure on the base plate of the cryostat, (6) to install the whole assembly of helical coils on the lower half of the supporting structure, (7) to install the upper half of the supporting structure and to weld the whole assembly, (8) to set the upper poloidal coils and to adjust the whole coils, (9) to remove the winding core and to assemble the inner parts of the plasma vacuum vessel and (10) to assemble the cryostat.

Quality control is important for a large system like LHD. We carried out various tests during both component and on-site construction periods, such as measurements of material properties, dimension tolerance check, voltage breakdown and leak test. Furthermore, we performed several proof tests to ensure the results of the sub-systems, for example, one of the IV coils was cooled-down and excited up to the nominal current with a testing cryostat and test facilities at NIFS [19].

3. COMMISSIONING

After machine assembly, we proceeded on commissioning, which was followed by the first plasma operation.

3.1. Vacuum pumping

The vacuum pumping system consists of two pumping units for the plasma vacuum vessel and for the cryostat for thermal isolation. The manifolds with diameters of 1.2 m, as shown in Fig. 1, and 0.8 m are connected to the plasma vacuum vessel and cryostat, respectively. The pump units for the plasma vacuum vessel are two cryogenic pumps with a pumping speed of 70 m^3/s for water, two

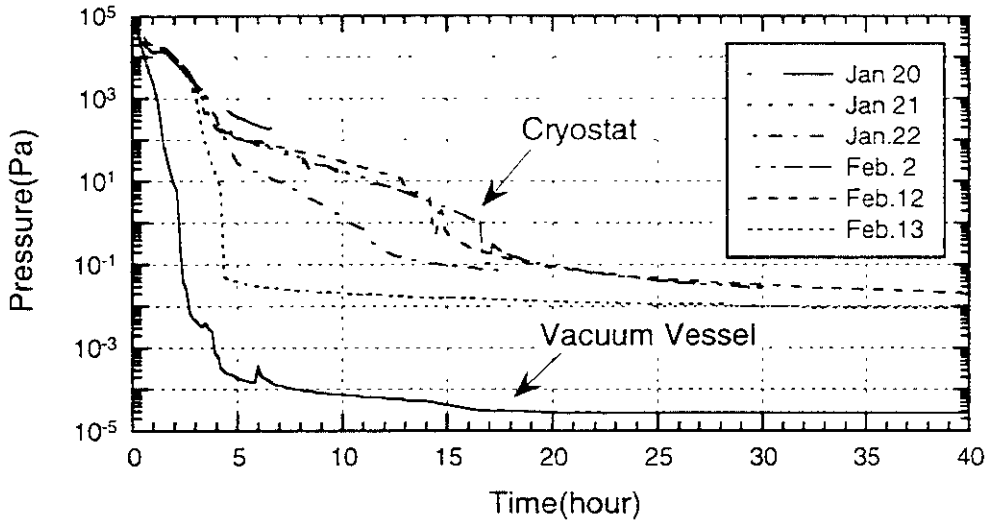

FIG. 3. Cryostat and plasma vacuum vessel pressures as a function of time.

turbomolecular pumps with a pumping speed of 5 m^3/s for nitrogen, two compound turbomolecular pumps with a pumping speed of 1.8 m^3/s for nitrogen, one mechanical booster pump with a pumping speed of 1,630 m^3/h and four rotary pumps with a pumping speed of 85 m^3/h. The pump units for the cryostat are two cryogenic pumps with a pumping speed of 25 m^3/s for water, two compound turbomolecular pumps with a pumping speed of 5.5 m^3/s for nitrogen, one mechanical booster pump with a pumping speed of 1,630 m^3/h and two rotary pumps with a pumping speed of 85 m^3/h. Two oil rotary pumps with a pumping speed of 900 m^3/h are used for first roughing.

The vacuum test of the cryostat began on January 20, 1998. The cryostat with the volume of 580 m^3 and an extended surface of about 70 km^2 was evacuated by introducing dry nitrogen for water vapor purge intermittently at 20 - 200 Pa up to 0.1 MPa. As shown in Fig. 3, we achieved the cryostat pressure of about 0.02 Pa within 3 1/2 days, which is low enough for the cool-down of LHD. The main species of the desorbed gas was found to be water, as expected. During the helium leak test a few small leaks were found in the helium cooling pipes that are located inside the cryostat. These were plugged in, and no leak has been left in the cryostat in the range 10^{-8} Pam^3/s. The vacuum test of the plasma vacuum vessel began on January 30. The pressure of the plasma vacuum vessel reached 3×10^{-5} Pa within a day, and no leak was found in the plasma vacuum vessel and water cooling pipes in the range 10^{-9} Pam^3/s. At the end of March, 1998, the pressure of the plasma vacuum vessel reached 9×10^{-7} Pa.

3.2. Cool-down

We started the main compressors on February 9, 1998, and continued purifying operation of the cryogenic system until February 22 to remove impurities in the helium gas, such as oxygen, nitrogen, water, etc., less than 2 ppm. The first cool-down of LHD started on February 23, and finished on March 22. Figure 4 shows the cooling curves of the helical and poloidal coils as well as the date of the transition to the superconducting state, indicated by the voltage drops of the coils at 10 A coil currents. At first, the superconducting coils, supporting structures and 80 K shield were cooled by helium gas, the temperature of which was controlled by mixing cold and warm gases in order to keep the temperature distribution in the coils and supporting structures less than 50 K. Thus, this temperature distribution determined the cooling rate. Below 85 K, 7 turbo-expanders were put to operation. The helical coils, poloidal coils and superconducting bus-lines have turned into

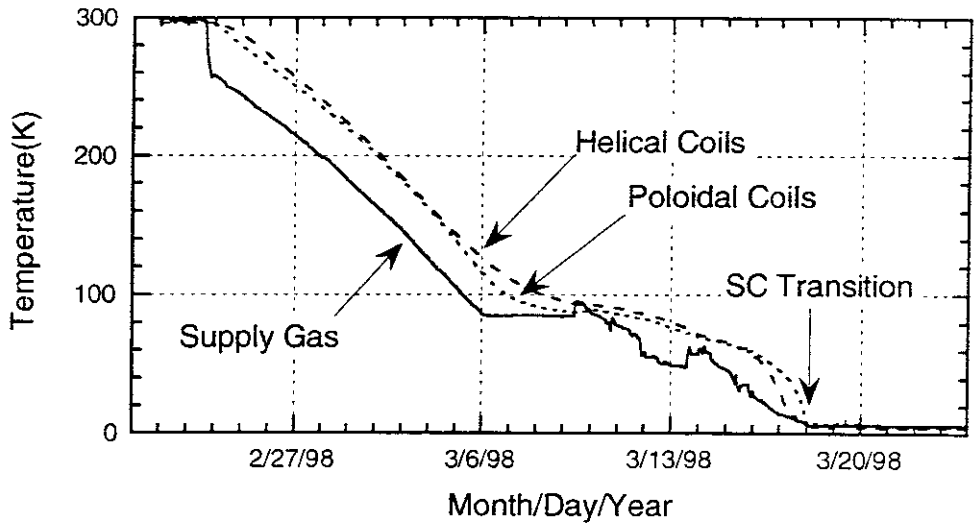

FIG. 4. Cool-down curves of helical and poloidal coils.

superconductors since March 18, when the supply gas temperature was 8.5 K and the coil outlet gas temperature was 9.0 K.

3.3. Field generation

After all the coils were completely cooled down and liquid helium was stored sufficiently, the first excitation test of superconducting coils was conducted. Through the process of debugging the control program and adjusting the feedback gain of current control in low currents, the coils were successfully excited up to 1.5 T without abnormal heat generation in the coils on March 27. The accuracy of current control did not reach the target value in the initial operation, but it was improved at the end of the first plasma experiment campaign [20].

4. INITIAL PLASMA EXPERIMENTS

4.1. Magnetic flux mapping

Magnetic flux mapping was done under steady-state conditions at reduced magnetic fields ranging up to 0.25 T, using the fluorescent method. In the measurements, an electron gun with a LaB6 cathode and a fluorescent mesh were used. The diameter of the electron beam was limited to less than 3 mm. The fluorescent mesh of 1 m × 2 m was located at the toroidal plane, the cross section of which is elongated vertically. The magnetic surfaces were measured by taking pictures of the beam images on the fluorescent mesh while changing the radial position of the electron gun. The pictures were taken with an intensified charge-coupled device (CCD) camera, which was aligned in parallel with the tangential port for the neutral beam injection.

Clear pictures of the magnetic surfaces were obtained, as shown in Fig. 5(a). It is quite obvious that there are closed, nested magnetic surfaces in good agreement with the theoretical calculation, as can be seen in Fig. 5(b). Figure 5(a) shows also the existence of a clear m/n = 1/1 island. This island is considered to be formed by the terrestrial magnetism, because the magnetic field was low when the mapping was performed. In Fig. 5(b), the magnetic surfaces were calculated taking into account the terrestrial magnetism, and demonstrating that the m/n = 1/1 and 2/1 islands

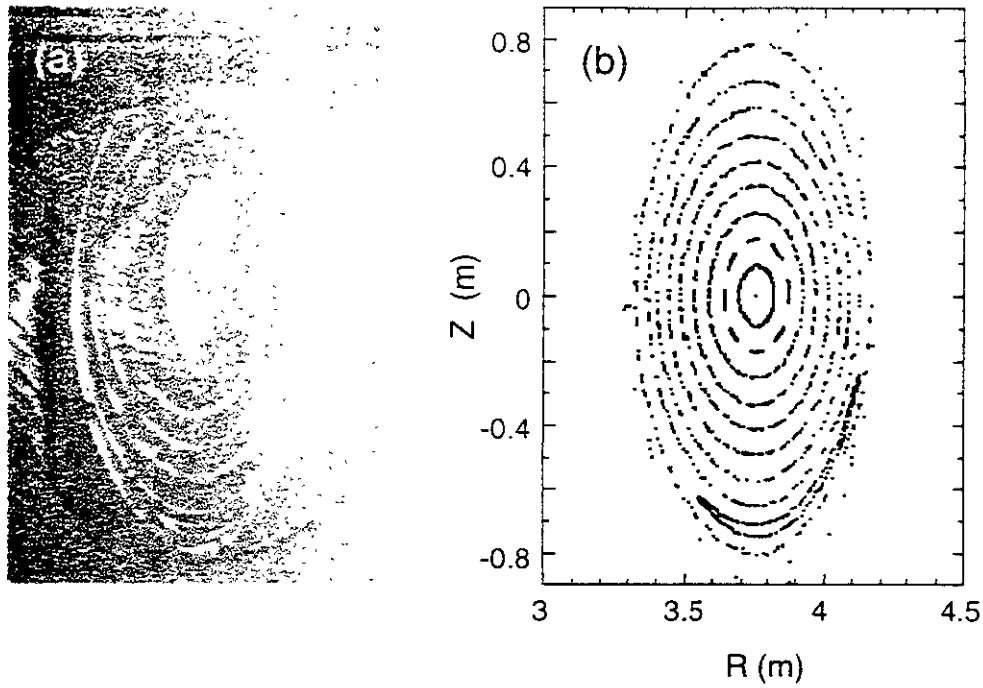

FIG. 5. (a) Measured and (b) calculated magnetic surfaces at B_t = 0.0875 T. In the calculation, the terrestrial magnetism is taken into account.

can be formed surely by the terrestrial magnetism at this low magnetic field. The calculated poloidal phases and maximum widths of the islands were found to agree well with those of the experimental results. The maximum width of the m/n = 1/1 island was reduced by a factor of about 1.3 when the mapping was performed at B_t = 0.25 T, compared with that at B_t = 0.0875 T. Even at this stage of the magnetic flux mapping studies, it is suggested that the accuracy in LHD's helical and poloidal coils and their alignment is better than the value required for LHD.

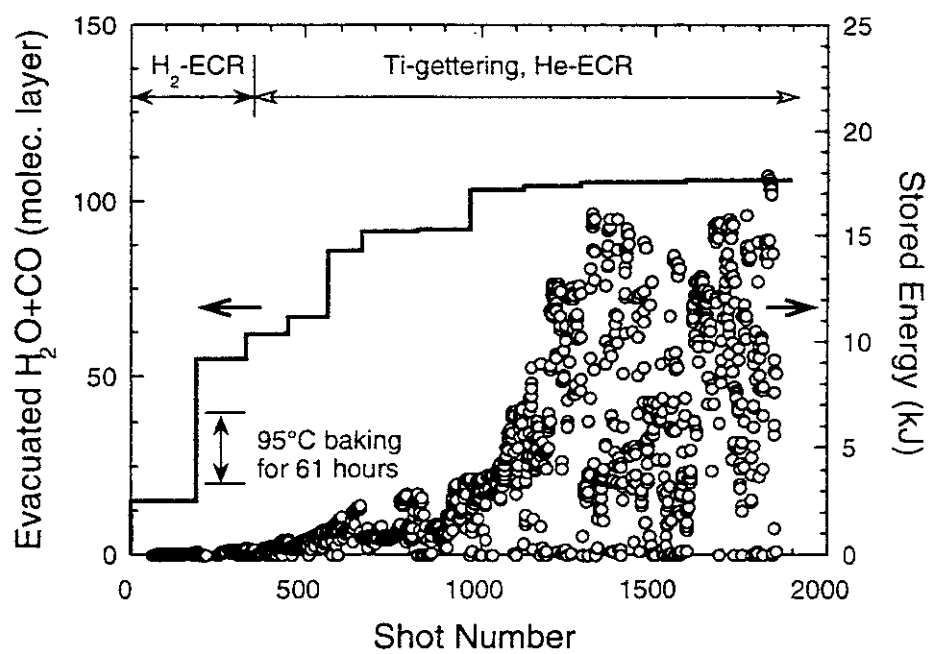

FIG. 6. Total amount of evacuated impurity gases and stored energy as a function of shot number in the first campaign.

4.2. Wall conditioning

Hydrogen discharge cleaning of the plasma vacuum vessel was done with the standard magnetic configuration of 875 G using the 2.45 GHz ECR system with the power of 10 kW. Then, the first plasma was produced with ECH of 150 kW on March 31. Baking the plasma vacuum vessel at temperatures around 95 °C was performed after the first plasma, and hydrogen and helium ECR discharge cleaning with the power of 5 kW was performed before and after Ti-gettering, respectively. The main desorbed gases were hydrogen, carbon monoxide and water. To enhance wall conditioning, the toroidally-distributed Ti-gettering was done once or twice a day, which covers a 20 - 30% plasma-facing wall surface.

Figure 6 shows the evolution of the plasma stored energy, W_p, and evacuated molecular layers as a function of shot number in the first campaign, demonstrating that W_p remarkably increased after the impurity gas was evacuated. The total amount of oxygen was about 100 molecular layers, that is, about 50g. At the end of the first campaign, W_p reached about 15 kJ. The electron temperature, T_e, also exceeded 1.3 keV and n_e was of the order of 5×10^{18} m^{-3}.

In the second campaign, after baking the plasma vacuum vessel for 240 hrs, helium glow discharge cleaning with the power of 5 kW, partly combined with helium ECR discharge cleaning, is curried out, including the conditioning of the NBI injection ports. This results in good wall conditioning, and more or less the same result as in the first campaign is obtained. After the high-power operation of NBI, glow discharge cleaning is effective on improving the wall condition.

4.3. ECH plasma

In the first campaign, continued to May 13, 1998, plasmas were produced by two gyrotrons. The total input power was 0.35 MW for the pulse duration of 0.25 - 0.5 s. It was found that an abrupt increase of n_e during start-up of plasma discharge is accompanied by the expansion of plasma

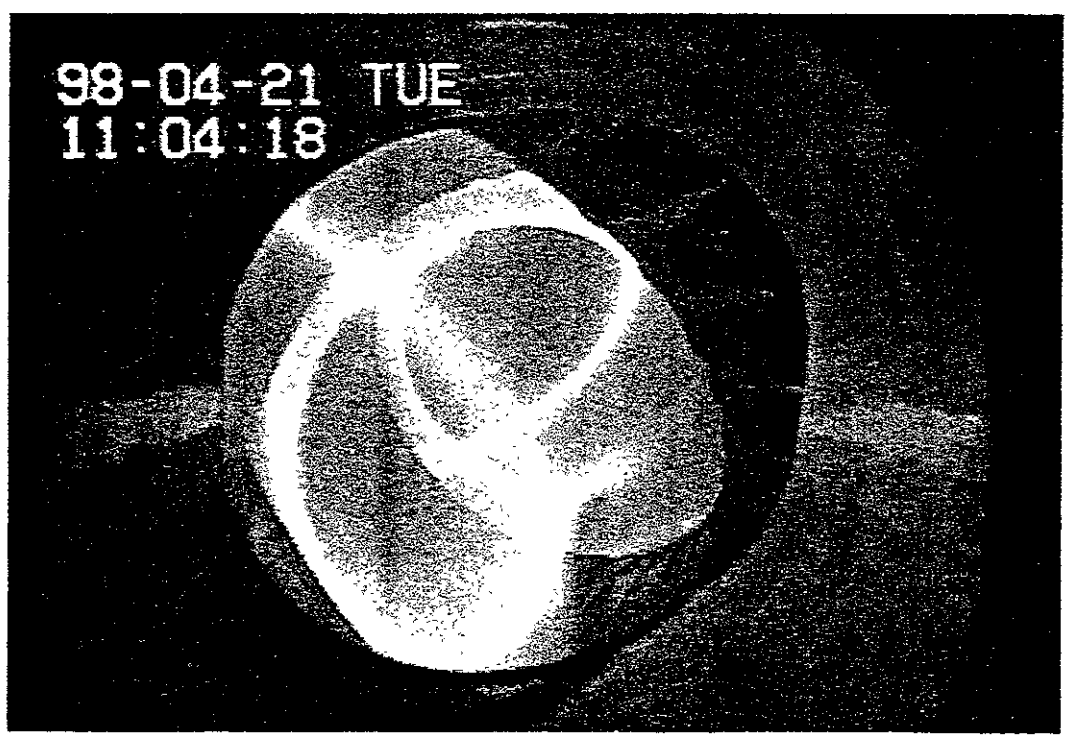

FIG. 7. TV image of the LHD plasma, which is well expanded.

volume. At first, the plasma is produced only about the resonance point, located at the plasma center, because the elliptical Gaussian beam of ECH is focused at the resonance point on the equatorial plane. Then, the plasma volume becomes large. Figure 7 shows a TV image of the plasma, which is well expanded and wrapped in a luminous layer. Time evolution of the plasma radius can be obtained by measuring the position of this luminous layer. The TV image also demonstrated that the plasma radius is changed by the balance of the input power and total amount of gases, puffed and released from the plasma vacuum wall. Diverted plasma flux profiles have been measured with a 30-channel array of Langmuir probes, located outside the X-point. Particle fluxes with high T_e of 20 eV, which were measured as the ion saturation currents, were detected at the same time that the luminous layer reached the divertor region, indicating good agreement with the time evolution of the TV image of the plasma. Furthermore, it was observed the well-defined profile of the ion saturation current with a half-maximum width of less than 10 mm. The peak positions agree well with the results of the magnetic field calculation within ±5 mm.

The plasma parameters achieved in the first campaign are summarized as follows: (1) T_e of 1.3 keV and n_e of 3×10^{18} m^{-3} at the ECH power of 270 kW; (2) n_e of 1.3×10^{19} m^{-3} at the ECH power of 80 kW; (3) energy confinement time, τ_E as long as 0.25 s at n_e of 6×10^{18} m^{-3} and the ECH power of 70 kW. Although the experiment was usually performed at a magnetic axis position, R_{ax}, of 3.75 m, data were also taken at R_{ax} = 3.9 m. The comparison between these data indicates that the better confinement is achieved at R_{ax} = 3.75 m, compared with that at R_{ax} = 3.9 m, as expected from the calculation of particle orbits.

A local island divertor (LID) experiment was performed using only the LID magnetic configuration, where an m/n = 1/1 island is generated by the twenty LID coils, to study the effect of the LID magnetic configuration on the ECH plasma. In the usual LID experiment, the outward heat and particle fluxes crossing the island separatrix flow along the field lines to the back side of the island, where target plates are placed on a divertor head [5, 6]. The particles recycled there are pumped, and hence, the geometrical shapes of the divertor head and pumping duct should be designed to form a closed divertor configuration with a high pumping efficiency [5]. The divertor head was, however, not used in the first campaign, because it was not constructed yet. We found that the plasma parameters change significantly when the plasma is not fully expanded. In this case, the radiation power, measured with a bolometer, and the OV and CIII radiation intensities decrease significantly in the LID magnetic configuration, while n_e decreases a little. The stored energy, W_p, measured by a diamagnetic loop, increases significantly, suggesting improved confinement. However, the plasma parameters little change when the plasma is fully expanded. This detailed analysis is under way in preparation for the next LID experiment.

Quasi steady-state operation with the duration of 140 s was attained at the end of the first campaign. An ECH pulse train of 80 kW/1 Hz /10% duty was injected into the plasma. Despite the fact that the power input is not truly continuous, an AC mode of operation has been achieved. During this AC plasma operation, impurities such as OV and CIII were also observed to keep track of the plasma density evolution.

4.4. Auxiliary heating plasmas

In the second campaign, two 84-GHz and one 82.6-GHz gyrotrons are used for producing a target plasma for NBI. The total input power of ECH is around 0.42 MW for the pulse duration of 0.25 - 0.4 s. In the ECH phase, n_e and W_p are measured to be 1.7×10^{19} m^{-3} and about 36 kJ, respectively. The ion sources of NBI are optimized for a low energy of 100 keV, considering that the target plasma density is low under the 1.5 T operation. In this case, the maximum injecting beam power is limited to 4 - 5 MW for 1 s.

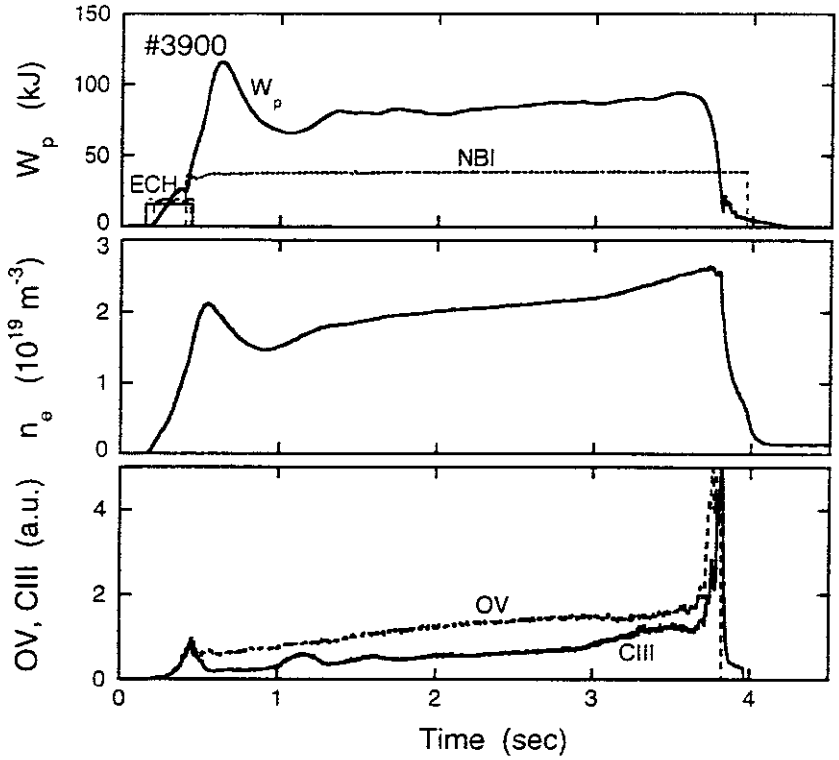

FIG. 8. Time evolution of stored energy, W_p, averaged electron density, n_e, OV radiation intensity and CIII radiation intensity.

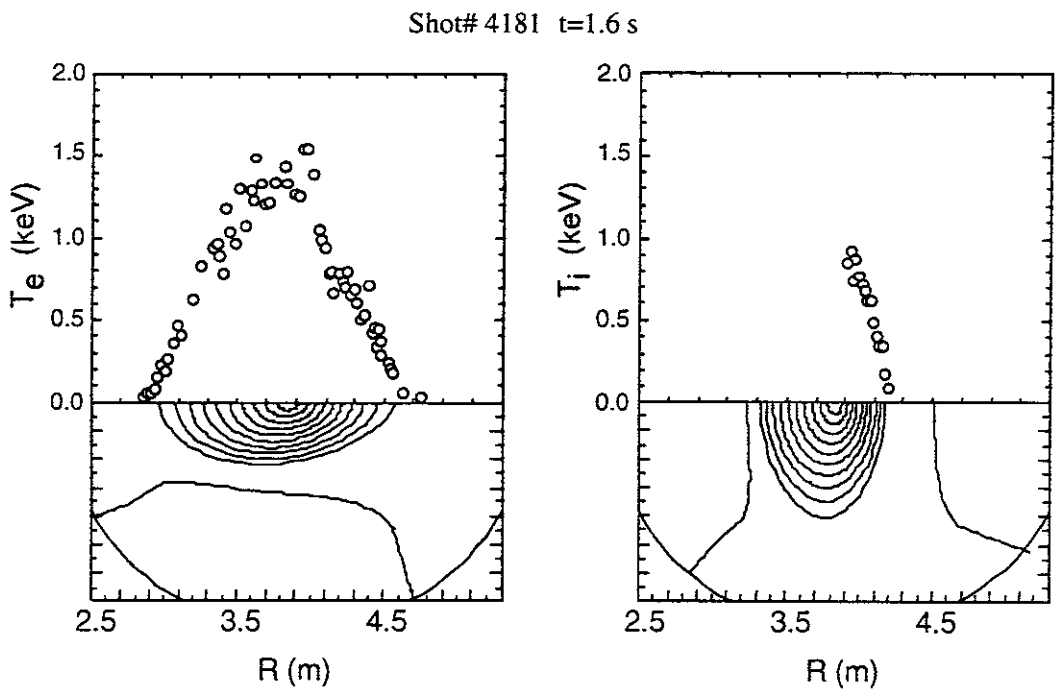

FIG. 9. Radial profiles of electron temperature, T_e, and ion temperature, T_i.

In the presence of NBI with the duration of less than 0.5 s, n_e in the hydrogen puffing discharge is found to decrease significantly and the diverted plasma flux increases during this pumping phase. LHD employs metal walls, that is, stainless-steel walls, and has no limiter. Thus, it

TABLE III. PLASMA PARAMETERS ATTAINED IN EXPERIMENTS

	T_e (keV)	T_i (keV)	τ_E (sec)	P_{abs} (MW)	n_e (10^{19} m^{-3})
High Temperature	1.5	1.1	0.11	1.6	1.5
	-	1.4	-	-	0.4
High Confinement	0.8	-	0.17	1.3	5.0
	Fusion Triple Product = 8×10^{18} keV m^{-3} sec				
Maximum Density					
	6.3×10^{19} m^{-3} (Helium gas puff)				
	6.0×10^{19} m^{-3} (Hydrogen pellet)				
Maximum Stored Energy					
	W_p = 0.22 MJ				
	$<\beta>$ = 0.7 % with 3 MW Port-through				

is considered that the metal wall strongly pump the hydrogen plasma and that a global recycling coefficient in LHD is less than unity. The increase in NBI power results in a shorter decay time of the density drop. The hydrogen-pellet injection experiment, performed for the purpose of fueling, shows also the large decrease of n_e after the sudden increase of n_e at the instant the pellet is injected. Because the wall is considered to be saturable, the investigation of longer discharges than 0.5 s has just started, controlling the gas puffing. By contrast, in helium discharges, where the helium gas puffing is performed while the beam species is hydrogen, the wall-pumping phenomenon becomes much milder, and n_e can be kept almost constant during the discharge with the duration of less than a few seconds.

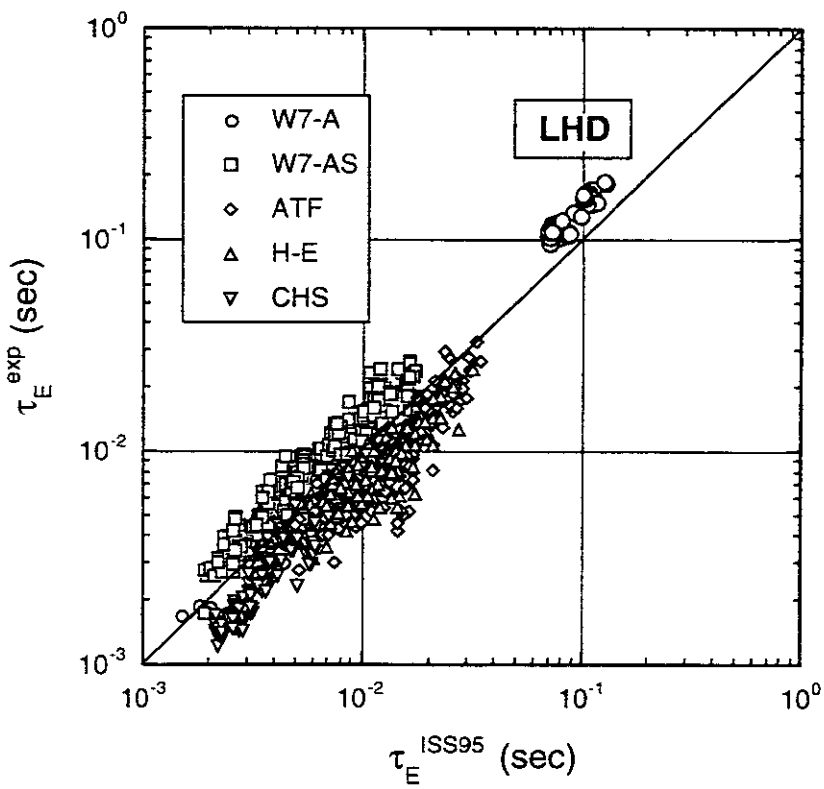

FIG. 10. Energy confinement time data vs. the ISS95 scaling law.

Time evolution of plasma parameters is shown in Fig. 8, obtained in the helium puffing discharge. The maximum duration of the discharge is about 10 s at this stage. The profiles of T_e and ion temperature, T_i, are shown in Fig. 9. It should be noted that T_i at the outermost flux surface reaches 300 eV, suggesting the feasibility of a high-temperature divertor operation, where a divertor plasma with a temperature of a few keV is produced, leading to a significant energy confinement improvement [21]. The plasma parameters attained in the hydrogen gas puffing are summarized in Table III; $n\tau T$ is 8×10^{18} keVm^{-3}s and $<\beta>$ is 0.7%. These are about one tenth of the goal values. The maximum T_i is 1.4 keV at low n_e of less than 4×10^{18} m^{-3}.

Fig. 10 depicts the energy confinement time, τ_E, and the ISS95 scaling law, $\tau_E^{ISS95} = 0.079a^{2.21}R^{0.65}B_t^{0.83}n_e^{0.51}P_{abs}^{-0.59}(\iota/2\pi)^{0.4}$, where P_{abs} and ι are the total absorbed power and rotational transform, respectively [22]. The energy confinement time, τ_E, was estimated by W_p measured by the diamagnetic loops. The response of the diamagnetic loops has been calculated by the 3-D magnetic field analysis with 3-D finite-β equilibrium. The NBI deposition profiles were evaluated using a Monte Carlo simulation code, MCNBI [23], and the ECH deposition power was derived from the water load measurement considering losses due to mirrors and bends in the wave guides. All data in Fig. 10 were taken at R_{ax} = 3.75 m during hydrogen gas puffing. We found that LHD's τ_E is clearly longer than the existing helical devices by about one order of magnitude and that τ_E is longer than τ_E^{ISS95}, representing better energy confinement than the ISS95 scaling law. Details on physics results are presented elsewhere [24].

The ICRF heating experiment also will start in the second campaign. One pair of fast wave antennas was installed for electron/ion heating. The expected loading power is 1 MW for 1s, and will be increased up to 2 MW for 10 s or 0.5 MW at steady state.

5. FUTURE PLANS

Figure 11 shows a near-term schedule of the LHD experiment. The excitation test to the rated field of 3 T is planned during this conference. From the third experimental campaign, experiments

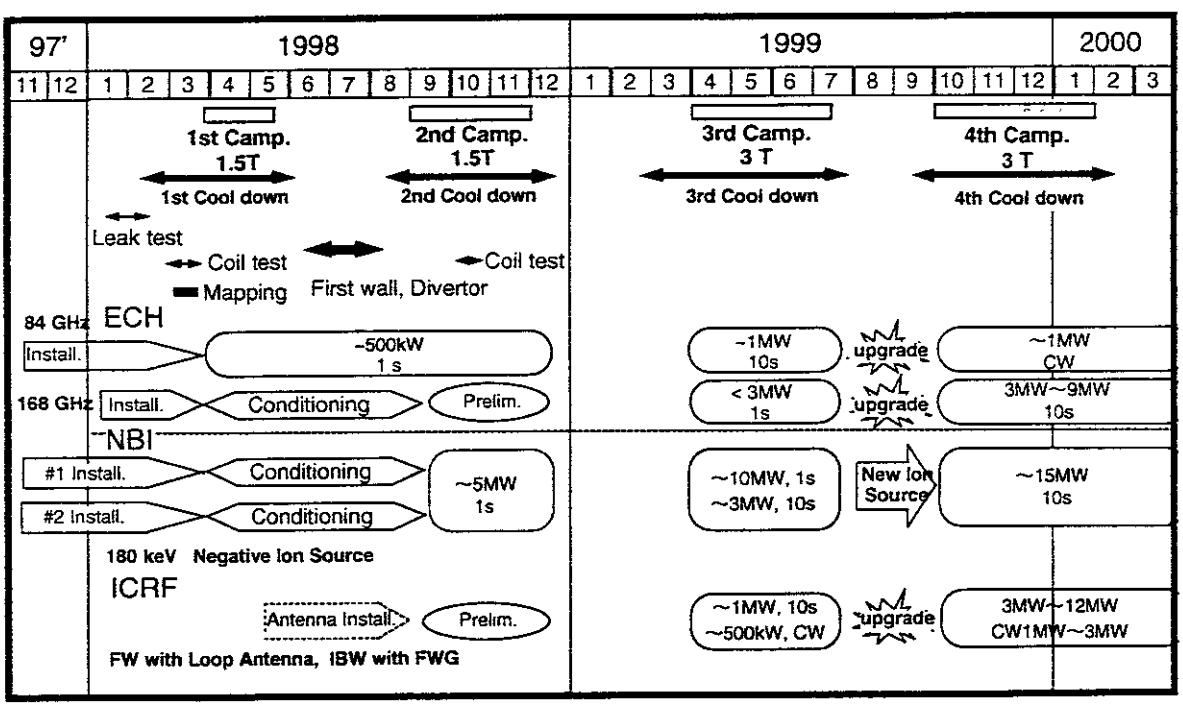

FIG. 11. Near-term scheme of LHD experiments.

will be conducted at B_t = 3 T with the heating power increased gradually The ECH power is planned to range from 3 to 10 MW. The beam energy of NBI will be increased up to 180 keV, and the injection power is raised up to 10 MW. For the full power operation at the heating power of 15 MW, the ion sources should be modified to reduce the electron component. For the ICRF heating experiments, a folded wave guide antenna will be installed before the next campaign for Ion Bernstein heating by which plasma production can be done independently of the magnetic field. The expected loading power is 1 MW for 1 s and will be increased up to 2 MW for 10 s. In the future we plan to install more antennas to increase the loading power up to 12 MW for 10 s or 3 MW at steady state.

For the edge plasma control, LID is tested in 1998 - 1999, and the divertor head will be installed in 1999 or in 2000. The steady-state operation at a 1 MW level is tried at first and gradually increased up to 3 MW, in parallel with the development of the heat removal method in 1998 - 2001 [25].

In the upgrade phase, that is, Phase-II, the magnetic field is increased to 4 T by 1.8 K operation of the helical coil. The full helical divertor equipped with baffle plates by which the closed divertor operation is possible will be installed, and D beams will be injected into D plasmas.

6. SUMMARY

After challenging technology R&D over the period of eight years, the construction of LHD has been completed recently. The first evacuation and cooling-down were performed, and the helical coils and poloidal coils successfully became superconductive. Auxiliary heating experiments with NBI of 3 MW have achieved the electron temperature of 1.5 keV and the ion temperature of 1.1 keV with the averaged electron density of 1.5×10^{19} m^{-3} at the magnetic field of 1.5 T. The ion temperature is 1.4 keV at the maximum. The maximum stored energy has reached 0.22 MJ, which corresponds to $\langle\beta\rangle = 0.7\%$. The energy confinement time data, exceeding 0.25 s at the maximum, have shown a similar manner of the present scaling law with some enhancement, which was derived from existing medium size helical devices.

From the third campaign, experiments will be conducted at the magnetic field of 3 T with the heating power increased gradually. We are aiming at achieving improved confinement in LHD like H-mode in tokamaks.

The goals of the LHD experiments are to understand the physics of steady-state currentless plasmas and to demonstrate the feasibility of heliotrons as the power reactor. In order that these goals are achieved, world-wide collaboration and participation in the LHD experiments are invited.

ACKNOWLEDGMENTS

Fusion research is based on the integration of plasma physics, fusion science and reactor engineering. The LHD project has been supported by many coworkers in these fields from universities, institutes and industries in Japan and throughout the world. We would like to thank all of these people for their contributions.

REFERENCES

[1] IIYOSHI, A., et al., Fusion Technol. **17** (1990) 169.
[2] MOTOJIMA, O., et al., in Plasma Physics and Controlled Nuclear Fusion Research 1990 (Proc. 13th Int. Conf. Washington, 1990) Vol. 3, IAEA, Vienna (1991) 513.
[3] YAMAZAKI, K., et al., in Plasma Physics and Controlled Nuclear Fusion Research 1990 (Proc. 13th Int. Conf. Washington, 1990) Vol. 2, IAEA, Vienna (1991) 709.
[4] FUJIWARA, M., et al., Plasma Phys. Control. Fusion **39** (1997) A261.
[5] KOMORI, A., et al., in Plasma Physics and Controlled Nuclear Fusion Research 1994 (Proc. 15th Int. Conf. Seville, 1994) Vol. 2, IAEA, Vienna (1995) 773.
[6] KOMORI, A., et al., in Fusion Energy 1996 (Proc. 16th Int. Conf. Montreal, 1996) Vol. 2, IAEA, Vienna (1997) 3.
[7] MOTOJIMA, O., et al., paper IAEA-F1-CN-69/FT2/1, this conference.
[8] MITO, T., et al., Fusion Eng. Des. **10** (1993) 233.
[9] YANAGI, N., et al., Advances in Cryogenic Eng. **40** (1994) 459.
[10] TAKAHATA, K., et al., Fusion Eng. Des., **20** (1993) 161.
[11] YAMADA, S., et al., IEEE Trans. on Magnets **32** (1996) 2422.
[12] SENBA, T., et al., in Fusion Technol. 1994 (Proc. 18th Int. Conf. Karlsruhe, 1994) Vol. 2, Elsevier Science. B. V., Amsterdam (1995) 905.
[13] NISHIMURA, A., et al., Proc. of Fusion Technology 1998, Marseilles, Vol. 1, p. 869.
[14] CHIKARAISHI, H., et al., Proc. of Power Conversion Conf. 1997, Nagaoka, p. 747.
[15] MITO, T., et al., Advances in Cryogenic Eng. **43** (1998), to be published.
[16] SUZUKI, H., et al., Transactions of Fusion Technol. **27** (1995) 523.
[17] SUZUKI, H., et al., J. Plasma Fusion Res. SERIES 1 (1998) 402.
[18] FUJITA, J., Fusion Eng. & Design **34&35** (1997) 11.
[19] SATOW, T., et al., Proc. of ICEC16/ICMC 1997, Kitakyusyu, 735.
[20] CHIKARAISHI, H., et al., Proc. of Fusion Technology 1998, Marseilles, Vol. 1, p. 759.
[21] OHYABU, N., et al., Nucl. Fusion **34** (1994) 387.
[22] STROTH, U., et al., Nucl. Fusion **36** (1996) 1063.
[23] MURAKAMI, S., et al., Trans. Fusion Tech. **27** (1995) 256.
[24] FUJIWARA, M., et al., paper IAEA-F1-CN-69/EX2/3, this conference.
[25] NODA, N., et al., Proc. of 11th Int. Stellarator Conf. 1997, LW-2.

Recent Issues of NIFS Series

NIFS-502 V Vdovin, T Watari and A Fukuyama,
An Option of ICRF Ion Heating Scenario in Large Helical Device, July 1997

NIFS-503 E Segre and S Kida,
Late States of Incompressible 2D Decaying Vorticity Fields, Aug 1997

NIFS-504 S Fujiwara and T Sato,
Molecular Dynamics Simulation of Structural Formation of Short Polymer Chains, Aug 1997

NIFS-505 S Bazdenkov and T Sato
Low-Dimensional Model of Resistive Interchange Convection in Magnetized Plasmas, Sep 1997

NIFS-506 H Kitauchi and S Kida,
Intensification of Magnetic Field by Concentrate-and-Stretch of Magnetic Flux Lines, Sep 1997

NIFS-507 R L Dewar,
Reduced form of MHD Lagrangian for Ballooning Modes, Sep. 1997

NIFS-508 Y.-N Nejoh,
Dynamics of the Dust Charging on Electrostatic Waves in a Dusty Plasma with Trapped Electrons, Sep 1997

NIFS-509 E Matsunaga, T Yabe and M. Tajima,
Baroclinic Vortex Generation by a Comet Shoemaker-Levy 9 Impact, Sep 1997

NIFS-510 C.C Hegna and N. Nakajima,
On the Stability of Mercier and Ballooning Modes in Stellarator Configurations, Oct. 1997

NIFS-511 K. Onto and T. Hatori,
Rotation and Oscillation of Nonlinear Dipole Vortex in the Drift-Unstable Plasma, Oct. 1997

NIFS-512 J. Uramoto,
Clear Detection of Negative Pionlike Particles from H_2 Gas Discharge in Magnetic Field; Oct 1997

NIFS-513 T Shimozuma, M Sato, Y Takita, S Ito, S Kubo, H. Idei, K Ohkubo, T Watari, T.S. Chu, K. Felch, P Cahalan and C.M Loring, Jr,
The First Preliminary Experiments on an 84 GHz Gyrotron with a Single-Stage Depressed Collector, Oct 1997

NIFS-514 T Shimozuma, S. Morimoto, M Sato, Y. Takita, S Ito, S Kubo, H Idei, K Ohkubo and T. Watari,
A Forced Gas-Cooled Single-Disk Window Using Silicon Nitride Composite for High Power CW Millimeter Waves; Oct. 1997

NIFS-515 K Akaishi,
On the Solution of the Outgassing Equation for the Pump-down of an Unbaked Vacuum System, Oct 1997

NIFS-516 *Papers Presented at the 6th H-mode Workshop (Seeon, Germany)*; Oct 1997

NIFS-517 John L. Johnson,
The Quest for Fusion Energy; Oct. 1997

NIFS-518 J Chen, N. Nakajima and M Okamoto,
Shift-and-Inverse Lanczos Algorithm for Ideal MHD Stability Analysis, Nov 1997

NIFS-519 M Yokoyama, N. Nakajima and M Okamoto,
Nonlinear Incompressible Poloidal Viscosity in L=2 Heliotron and Quasi-Symmetric Stellarators, Nov 1997

NIFS-520 S. Kida and H Miura,
Identificaiton and Analysis of Vortical Structures; Nov. 1997

NIFS-521 K. Ida, S. Nishimura, T Minami, K. Tanaka, S Okamura, M. Osakabe, H. Idei, S. Kubo, C. Takahashi and K. Matsuoka,

High Ion Temperature Mode in CHS Heliotron/torsatron Plasmas; Nov. 1997

NIFS-522 M. Yokoyama, N. Nakajima and M. Okamoto,
Realization and Classification of Symmetric Stellarator Configurations through Plasma Boundary Modulations; Dec. 1997

NIFS-523 H. Kitauchi,
Topological Structure of Magnetic Flux Lines Generated by Thermal Convection in a Rotating Spherical Shell; Dec. 1997

NIFS-524 T. Ohkawa,
Tunneling Electron Trap; Dec. 1997

NIFS-525 K. Itoh, S.-I Itoh, M. Yagi, A. Fukuyama,
Solitary Radial Electric Field Structure in Tokamak Plasmas; Dec. 1997

NIFS-526 Andrey N. Lyakhov,
Alfven Instabilities in FRC Plasma; Dec. 1997

NIFS-527 J. Uramoto,
Net Current Increment of negative Muonlike Particle Produced by the Electron and Positive Ion Bunch-method; Dec. 1997

NIFS-528 Andrey N. Lyakhov,
Comments on Electrostastic Drift Instabilities in Field Reversed Configuraiton, Dec. 1997

NIFS-529 J. Uramoto,
Pair Creation of Negative and Positive Pionlike (Muonlike) Particle by Interaction between an Electron Bunch and a Positive Ion Bunch; Dec. 1997

NIFS-530 J. Uramoto,
Measuring Method of Decay Time of Negative Muonlike Particle by Beam Collector Applied RF Bias Voltage; Dec. 1997

NIFS-531 J. Uramoto,
Confirmation Method for Metal Plate Penetration of Low Energy Negative Pionlike or Muonlike Particle Beam under Positive Ions; Dec. 1997

NIFS-532 J. Uramoto,
Pair Creations of Negative and Positive Pionlike (Muonlike) Particle or K Mesonlike (Muonlike) Particle in H2 or D2 Gas Discharge in Magnetic Field; Dec. 1997

NIFS-533 S. Kawata, C. Boonmee, T. Teramoto, L. Drska, J. Limpouch, R. Liska, M Sinor,
Computer-Assisted Particle-in-Cell Code Development; Dec. 1997

NIFS-534 Y. Matsukawa, T. Suda, S. Ohnuki and C. Namba,
Microstructure and Mechanical Property of Neutron Irradiated TiNi Shape Memory Alloy; Jan. 1998

NIFS-535 A. Fujisawa, H. Iguchi, H. Idei, S. Kubo, K Matsuoka, S Okamura, K Tanaka, T Minami, S. Ohdachi, S. Morita, H Zushi, S. Lee, M. Osakabe, R. Akiyama, Y. Yoshimura, K. Toi, H. Sanuki, K. Itoh, A. Shimizu, S. Takagi, A. Ejiri, C. Takahashi, M. Kojima, S. Hidekuma, K Ida, S. Nishimura, N. Inoue, R. Sakamoto, S.-I. Itoh, Y Hamada, M. Fujiwara,
Discovery of Electric Pulsation in a Toroidal Helical Plasma, Jan. 1998

NIFS-536 Lj.R. Hadzievski, M.M. Skoric, M. Kono and T. Sato,
Simulation of Weak and Strong Langmuir Collapse Regimes; Jan 1998

NIFS-537 H. Sugama, W. Horton,
Nonlinear Electromagnetic Gyrokinetic Equation for Plasmas with Large Mean Flows; Feb. 1998

NIFS-538 H. Iguchi, T.P. Crowley, A. Fujisawa, S. Lee, K. Tanaka, T. Minami, S. Nishimura, K. Ida, R. Akiyama, Y Hamada, H., Idei. M. Isobe, M. Kojima, S. Kubo, S. Monta, S. Ohdachi, S. Okamura, M. Osakabe, K. Matsuoka, C. Takahashi and K. Toi,
Space Potential Fluctuations during MHD Activities in the Compact Helical System (CHS); Feb. 1998

NIFS-539 Takashi Yabe and Yan Zhang,
Effect of Ambient Gas on Three-Dimensional Breakup in Coronet Formation Process; Feb. 1998

NIFS-540 H Nakamura, K Ikeda and S Yamaguchi,
Transport Coefficients of InSb in a Strong Magnetic Field Feb 1998

NIFS-541 J Uramoto,
Development of ν_μ Beam Detector and Large Area ν_μ Beam Source by H_2 Gas Discharge (I), Mar. 1998

NIFS-542 J Uramoto,
Development of $bar\{\nu\}_\mu$ Beam Detector and Large Area $bar\{\nu\}_\mu$ Beam Source by H_2 Gas Discharge (II), Mar 1998

NIFS-543 J Uramoto,
Some Problems inside a Mass Analyzer for Pions Extracted from a H_2 Gas Discharge; Mar 1998

NIFS-544 J Uramoto,
Simplified ν_μ $bar\{\nu\}_\mu$ Beam Detector and ν_μ $bar\{\nu\}_\mu$ Beam Source by Interaction between an Electron Bunch and a Positive Ion Bunch; Mar 1998

NIFS-545 J Uramoto,
Various Neutrino Beams Generated by D_2 Gas Discharge; Mar 1998

NIFS-546 R. Kanno, N Nakajima, T Hayashi and M. Okamoto,
Computational Study of Three Dimensional Equilibria with the Bootstrap Current; Mar 1998

NIFS-547 R. Kanno, N. Nakajima and M. Okamoto,
Electron Heat Transport in a Self-Similar Structure of Magnetic Islands; Apr. 1998

NIFS-548 J.E Rice,
Simulated Impurity Transport in LHD from MIST; May 1998

NIFS-549 M.M Skoric, T Sato, A.M. Maluckov and M S. Jovanovic,
On Kinetic Complexity in a Three-Wave Interaction; June 1998

NIFS-550 S Goto and S. Kida,
Passive Saclar Spectrum in Isotropic Turbulence: Prediction by the Lagrangian Direct-interaction Approximation; June 1998

NIFS-551 T Kuroda, H Sugama, R Kanno, M. Okamoto and W. Horton,
Initial Value Problem of the Toroidal Ion Temperature Gradient Mode ; June 1998

NIFS-552 T Mutoh, R. Kumazawa, T Seki, F. Simpo, G. Nomura, T Ido and T Watari,
Steady State Tests of High Voltage Ceramic Feedthoughs and Co-Axial Transmission Line of ICRF Heating System for the Large Helical Device ; June 1998

NIFS-553 N Noda, K Tsuzuki, A. Sagara, N Inoue, T Muroga,
oronaization in Future Devices -Protecting Layer against Tritium and Energetic Neutrals-: July 1998

NIFS-554 S. Murakami and H. Saleem,
Electromagnetic Effects on Rippling Instability and Tokamak Edge Fluctuations; July 1998

NIFS-555 H. Nakamura , K. Ikeda and S. Yamaguchi,
Physical Model of Nernst Element; Aug. 1998

NIFS-556 H. Okumura, S Yamaguchi, H. Nakamura, K Ikeda and K Sawada,
Numerical Computation of Thermoelectric and Thermomagnetic Effects, Aug 1998

NIFS-557 Y Takeiri, M Osakabe, K. Tsumori, Y. Oka, O. Kaneko, E Asano, T Kawamoto, R. Akiyama and M Tanaka,
Development of a High-Current Hydrogen-Negative Ion Source for LHD-NBI System, Aug.1998

NIFS-558 M. Tanaka, A. Yu Grosberg and T. Tanaka,
Molecular Dynamics of Structure Organization of Polyampholytes; Sep. 1998

NIFS-559 R Horiuchi, K Nishimura and T. Watanabe,

Kinetic Stabilization of Tilt Disruption in Field-Reversed Configurations; Sep. 1998
(IAEA-CN-69/THP1/11)

NIFS-560 S. Sudo, K. Kholopenkov, K. Matsuoka, S Okamura, C. Takahashi, R. Akiyama, A. Fujisawa, K. Ida, H. Idei, H Iguchi, M. Isobe, S Kado, K. Kondo, S. Kubo, H. Kuramoto, T. Minami, S. Morita, S. Nishimura, M Osakabe, M. Sasao, B. Peterson, K. Tanaka, K. Toi and Y. Yoshimura,
Particle Transport Study with Tracer-Encapsulated Solid Pellet Injection; Oct. 1998
(IAEA-CN-69/EXP1/18)

NIFS-561 A. Fujisawa, H. Iguchi, S. Lee, K. Tanaka, T Minami, Y. Yoshimura, M. Osakabe, K Matsuoka, S. Okamura, H Idei, S. Kubo, S Ohdachi, S. Morita, R. Akiyama, K. Toi, H. Sanuki, K. Itoh, K. Ida, A. Shimizu, S. Takagi, C. Takahashi, M. Kojima, S. Hidekuma, S. Nishimura, M. Isobe, A. Ejiri, N. Inoue, R. Sakamoto, Y. Hamada and M. Fujiwara,
Dynamic Behavior Associated with Electric Field Transitions in CHS Heliotron/Torsatron, Oct. 1998
(IAEA-CN-69/EX5/1)

NIFS-562 S. Yoshikawa,
Next Generation Toroidal Devices; Oct 1998

NIFS-563 Y. Todo and T. Sato,
Kinetic-Magnetohydrodynamic Simulation Study of Fast Ions and Toroidal Alfvén Eigenmodes; Oct. 1998
(IAEA-CN-69/THP2/22)

NIFS-564 T. Watari, T. Shimozuma, Y. Takeiri, R. Kumazawa, T. Mutoh, M. Sato, O. Kaneko, K. Ohkubo, S. Kubo, H. Idei, Y. Oka, M Osakabe, T Seki, K. Tsumori, Y. Yoshimura, R. Akiyama, T. Kawamoto, S. Kobayashi, F Shimpo, Y. Takita, E Asano, S Itoh, G Nomura, T Ido, M. Hamabe, M. Fujiwara, A. Iiyoshi, S Morimoto, T Bigelow and Y.P Zhao,
Steady State Heating Technology Development for LHD, Oct. 1998
(IAEA-CN-69/FTP/21)

NIFS-565 A Sagara, K.Y Watanabe, K. Yamazaki, O Motojima, M Fujiwara, O. Mitarai, S. Imagawa, H. Yamanishi, H Chikaraishi, A Kohyama, H. Matsui, T Muroga, T Noda, N Ohyabu, T Satow, A.A Shishkin, S. Tanaka, T. Terai and T. Uda,
LHD-Type Compact Helical Reactors; Oct. 1998
(IAEA-CN-69/FTP/03(R)

NIFS-566 N. Nakajima, J. Chen, K. Ichiguchi and M. Okamoto,
Global Mode Analysis of Ideal MHD Modes in L=2 Heliotron/Torsatron Systems; Oct 1998
(IAEA-CN-69/THP1/08)

NIFS-567 K. Ida, M. Osakabe, K. Tanaka, T. Minami, S. Nishimura, S. Okamura, A. Fujisawa, Y Yoshimura, S. Kubo, R. Akiyama, D.S.Darrow, H. Idei, H. Iguchi, M. Isobe, S. Kado, T. Kondo, S. Lee, K. Matsuoka, S. Morita, I. Nomura, S. Ohdachi, M. Sasao, A. Shimizu, K. Tumori, S Takayama, M. Takechi, S. Takagi, C. Takahashi, K. Toi and T Watari,
Transition from L Mode to High Ion Temperature Mode in CHS Heliotron/Torsatron Plasmas; Oct 1998
(IAEA-CN-69/EX2/2)

NIFS-568 S Okamura, K. Matsuoka, R. Akiyama, D.S Darrow, A. Ejiri, A. Fujisawa, M. Fujiwara, M Goto, K. Ida H. Idei, H. Iguchi, N Inoue, M. Isobe, K. Itoh, S. Kado, K. Khlopenkov, T. Kondo, S. Kubo, A. Lazaros, S. Lee, G. Matsunaga, T. Minami, S. Morita, S. Murakami, N. Nakajima, N. Nikai, S. Nishimura, I. Nomura, S. Ohdachi, K. Ohkuni, M Osakabe, R Pavlichenko, B. Peterson, R. Sakamoto, H. Sanuki, M. Sasao, A. Shimizu, Y. Shirai, S Sudo, S. Takagi, C. Takahashi, S. Takayama, M. Takechi, K Tanaka, K. Toi, K. Yamazaki, Y. Yoshimura and T Watari,
Confinement Physics Study in a Small Low-Aspect-Ratio Helical Device CHS, Oct 1998
(IAEA-CN-69/OV4/5)

NIFS-569 M.M. Skoric, T Sato, A. Maluckov, M.S. Jovanovic,
Micro- and Macro-scale Self-organization in a Dissipative Plasma: Oct. 1998

NIFS-570 T. Hayashi, N. Mizuguchi, T-H. Watanabe, T. Sato and the Complexity Simulation Group,
Nonlinear Simulations of Internal Reconnection Event in Spherical Tokamak; Oct 1998
(IAEA-CN-69/TH3/3)

NIFS-571 A. Iiyoshi, A. Komori, A. Ejiri, M. Emoto, H. Funaba, M. Goto, K. Ida, H Idei, S. Inagaki, S Kado, O. Kaneko, K. Kawahata, S. Kubo, R. Kumazawa, S. Masuzaki, T. Minami, J. Miyazawa, T. Morisaki, S. Morita, S. Murakami, S Muto, T Muto, Y Nagayama, Y. Nakamura, H Nakanishi, K. Narihara, K. Nishimura, N. Noda, T Kobuchi, S Ohdachi, N. Ohyabu, Y. Oka, M Osakabe, T. Ozaki, B.J. Peterson, A. Sagara, S. Sakakibara, R. Sakamoto, H. Sasao, M. Sasao, K. Sato, M. Sato, T. Seki, T. Shimozuma, M. Shoji, H. Suzuki, Y. Takeiri, K. Tanaka, K. Toi, T. Tokuzawa, K. Tsumori, I. Yamada, H. Yamada, S. Yamaguchi, M. Yokoyama, K.Y.Watanabe, T. Watari, R. Akiyama, H. Chikaraishi, K. Haba, S. Hamaguchi, S. Iima, S. Imagawa, N. Inoue, K. Iwamoto, S. Kitagawa, Y. Kubota, J. Kodaira, R. Maekawa, T. Mito. T. Nagasaka, A. Nishimura, Y. Takita, C. Takahashi, K. Takahata, K. Yamauchi, H. Tamura, T. Tsuzuki, S. Yamada, N. Yanagi, H. Yonezu, Y. Hamada, K. Matsuoka, K. Murai, K. Ohkubo, I. Ohtake, M. Okamoto, S. Sato, T Satow, S. Sudo, S. Tanahashi, K. Yamazaki, M. Fujiwara and O. Motojima,
An Overview of the Large Helical Device Project; Oct 1998
(IAEA-CN-69/OV1/4)